

# Latex-based concept for the preparation of graphene-based polymer nanocomposites

Evgeniy Tkalya,<sup>a</sup> Marcos Ghislandi,<sup>b</sup> Alexander Alekseev,<sup>b</sup> Cor Koning<sup>a</sup> and Joachim Loos<sup>\*b</sup>

Received 29th October 2009, Accepted 27th January 2010

First published as an Advance Article on the web 1st March 2010

DOI: 10.1039/b922604d

The latex technology concept is applied for the preparation of graphene/polystyrene nanocomposites. Aqueous dispersions of graphene are obtained *via* oxidation and exfoliation of graphite and subsequent reduction in the presence of surfactant. The quality of the prepared nanofillers is characterized by atomic force microscopy (AFM). Different amounts of aqueous graphene dispersions are then mixed with polystyrene (PS) latex and composites are prepared by freeze-drying and subsequent compression molding. The final bulk and local conductivities of the composites are respectively measured by a four-point method and by means of conductive AFM (C-AFM) analysis. The morphology of the conductive nanocomposites is studied with charge contrast scanning electron microscopy imaging (SEM). The percolation threshold for conduction is below 1 wt% of graphene in the composites, and a maximum conductivity of about 15 S m<sup>-1</sup> can be achieved for 1.6–2 wt% nanofiller.

## Introduction

Graphene (Gr) was first described as monocrystalline graphitic films which are a few atomic layers thick but are nonetheless of remarkably high quality and stable under ambient conditions.<sup>1</sup> It has attracted numerous investigators to study its unique physical, chemical, and mechanical properties, opening up a new research area for materials science.<sup>1–6</sup> Graphene can be obtained from cheap graphite by a simple chemical treatment such as oxidation followed by reduction using agents such as hydroquinone,<sup>1</sup> NaBH<sub>4</sub>,<sup>7,8</sup> dimethylhydrazine<sup>4</sup> and hydrazine,<sup>9</sup> and its cost could be lower than that of *e.g.* multiwall carbon nanotubes and much lower than that of single wall carbon nanotubes. Compared with carbon nanotubes (CNTs), which can be regarded as rolled-up graphene sheets, and accordingly are one-dimensional (1D), the corresponding graphene sheets are two-dimensional (2D), but have aspect ratios similar to those of the corresponding nanotubes. Electron transport in graphene is essentially governed by Dirac's (relativistic) equation. The charge carriers in graphene mimic relativistic particles with zero rest mass and have an effective 'speed of light'. All the induced carriers are mobile and there are no trapped charges in graphene.<sup>10</sup> Moreover sheet charge carriers can more easily bypass point defects of the sheet structure in comparison to 1D systems, which makes the charge transport in these 2D systems less sensitive to chemical treatments.<sup>9,11–13</sup> Graphene-based nanocomposites, with unique mechanical, electrical and dielectrical properties, could find use as engineering plastics and coatings, and could play a role as semi-conductive sheets in transistors.

Preliminary work in the latter field has shown some promising results.<sup>14–16</sup>

Despite potential advantages there are relatively few reports concerning graphene-based nanocomposites. Latex technology has already been applied for the incorporation of carbon nanotubes into a polymer matrix,<sup>17–20</sup> but thus far not for manufacturing polymer/graphene nanocomposites. This latex concept enables to incorporate nanofillers into any kind of highly viscous polymer such as PS, which can be synthesized by emulsion polymerization or similar processes.<sup>18,19</sup>

In this study, graphene/polystyrene (Gr/PS) nanocomposites were fabricated using latex technology and characterized with respect to morphology and conductivity properties.

## Experimental

### Chemicals

Sodium dodecyl sulfate (SDS) (90%, Merck), sodium carbonate (SC) (99%, Aldrich), sodium peroxodisulfate (SPS) (90%, Merck) and poly(styrene sulfonate) (PSS) (Aldrich, Mw 70 000 g mol<sup>-1</sup>) were used as received. Styrene (99%, Merck) was passed over an inhibitor remover column. The inhibitor-free monomers were kept under refrigeration for later use. Water used in all reactions was double de-ionized water obtained from a purification system. SP-2 graphite from Bay Carbon was used as filler.

### Preparation and characterization of PS latex

PS latex was synthesized *via* conventional free radical emulsion polymerization. The reaction was performed at 70 °C with an impeller speed of 400 rpm. The reactor was charged with the following: styrene (252 g), SDS (26 g, 0.09 mol), SC (0.7 g, 6.6 mmol) and H<sub>2</sub>O (712.2 g). The reaction mixture was degassed, by purging with argon, for 30 min. A solution of SPS (0.45 g, 1.9 mmol) in H<sub>2</sub>O (10 g) was also degassed. The reaction was started upon the introduction of the initiator solution, and

<sup>a</sup>Department of Polymer Chemistry, Technische Universiteit Eindhoven, 5600 MB Eindhoven, The Netherlands. E-mail: c.e.koning@tue.nl; Fax: +31 40 246 3966; Tel: +31 40 247 5353

<sup>b</sup>Laboratory of Materials and Interface Chemistry, Technische Universiteit Eindhoven, 5600 MB Eindhoven, The Netherlands. E-mail: j.loos@tue.nl; Fax: +31 40 244 5619; Tel: +31 40 247 3034

the reaction time was roughly 1 h. The average particle size determined by dynamic light scattering was 90 nm. Size exclusion chromatography analysis showed Mn, Mw and PDI values of 495 kg mol<sup>-1</sup>, 944 kg mol<sup>-1</sup> and 1.9, respectively.

### Gr/PS composites processing

Graphene was synthesized *via* oxidation of graphite (Hummers method),<sup>21</sup> followed by ultrasonication and subsequent reduction following the method described by Stankovich *et al.*<sup>9</sup> The oxidation of graphite to graphite oxide was accomplished by treating graphite with essentially a water-free mixture of concentrated sulfuric acid, sodium nitrate and potassium permanganate.<sup>21</sup> The entire process requires about three hours for completion. The obtained graphite oxide was exfoliated in order to generate graphene oxide sheets by tip sonication with a horn sonicator Sonic Vibracell VC750 with a cylindrical tip (13 mm end cap diameter). The frequency was fixed at (20 ± 2.0) kHz with an amplitude of 30%. The sheets were reduced for 72 h with hydrazine at 120 °C in the presence of a ten-fold excess (wt/wt) of PSS.<sup>9</sup> After its preparation, graphene covered with PSS was filtered off and dried under vacuum. The final PSS content (30%) was determined by elemental analysis. The product was then redispersed in water by a 40 min sonication process and then mixed with PS latex, the mixture was frozen in liquid nitrogen for several minutes and the frozen water was removed with a Christ Alpha 2–4 freeze dryer operated at 0.2 mbar and 20 °C overnight. The resulting composite powder was compression molded into films for 20 min at 180 °C between Teflon sheets with a Collin Press 300G.

### UV–Vis spectroscopic measurements

UV–Vis absorption spectra were recorded with a Hewlett–Packard 8453 spectrometer operating between 200 and 1100 nm, following a procedure described in the literature for carbon nanotube dispersions.<sup>24,25</sup> Small sample volumes (about 30 μl each, thus the sonicated volume under investigation is almost unchanged during the whole experiment) were taken regularly during the second sonicating process of the reduced graphene loaded with PSS (see Fig. 3) and diluted, resulting in a graphene concentration of 0.03 mg ml<sup>-1</sup>. The blank used was the original PSS solution, diluted and analyzed under the same conditions as the samples themselves.

### Electrical conductivity measurements

The electrical conductivity was measured using a standard four-point method. Parallel contact lines 1 cm in length and with a 1 cm interval were drawn with conductive-silver paint (Fluka) on the composite film, and all conductivity measurements were performed at room temperature with a Keithley 6512 programmable electrometer. For each sample, conductivity data represent the average value of 10 consecutive measurements.

### Scanning electron microscopy analyses

The images of Gr/PS composite films were obtained with a Quanta 3D FEG (Fei Co.) equipped with a field emission electron source. High vacuum conditions were applied and

a secondary electron detector was used for image acquisition. No additional sample treatment, such as surface etching or coating with a conductive layer, has been applied before surface scanning. Standard acquisition conditions for charge contrast imaging were used.<sup>22</sup>

### Atomic force microscopy (AFM) investigations

AFM characterization of graphite oxide platelets was performed with a Nanoscope 3A instrument (Veeco) operated in normal tapping mode. The substrate used for filler deposition was mica. The conductive AFM (C-AFM) measurements on composites cross sections were performed by an NTEGRA Tomo (NT-MDT Co.). The device is a combination of a microtome EM UC6-NT (Leica) and an SPM measuring head. Such design allows for alternate microtome cutting and SPM measurements of the sample block-face.<sup>26</sup> The local current measurements were performed in C-AFM mode with a gold-coated silicon cantilever NSC36/Cr-Au (Micromash). The sample was electrically connected to a grounded holder; a bias of 2 V was applied.

## Results and discussion

Graphite oxide produced by Hummers<sup>21</sup> method (see experimental part) has a layered structure. It was readily exfoliated in water by a gentle sonication process at a concentration of 1 mg ml<sup>-1</sup>. Most of the graphite oxide platelets analyzed exhibit a thickness below 1 nm, corresponding to 2–3 atomic layers, which clearly indicates the successful exfoliation driven by sonication (Fig. 1). There is always a compromise between the sonication time and the final graphene surface area and surface/thickness ratio, which is obtained after reduction of the graphite oxide. The optimum sonication time in order to prevent extensive breaking and destruction of the sheets, but still providing good exfoliation, was found to be 12–15 min. The average surface area of the graphite oxide platelets ranged from 1 to 3 μm<sup>2</sup>.

Reduction of graphite oxide with hydrazine at 120 °C in the presence of PSS resulted in a stable dispersion of graphene nanoplatelets in water. After filtering, the graphene covered with PSS could be easily redispersed in water (1 mg ml<sup>-1</sup>) by a second ultrasound treatment, remaining stable for a few days, after which some sedimentation occurred. Elemental analysis showed that the graphene/PSS ratio after filtering was 70/30 (wt/wt). The reduction of graphite oxide was carried out for 72 h, since electrical measurements of ‘buckypapers’ (graphene/PSS films prepared by vacuum filtration), indicated differences in conductivity depending on reduction time, probably due to

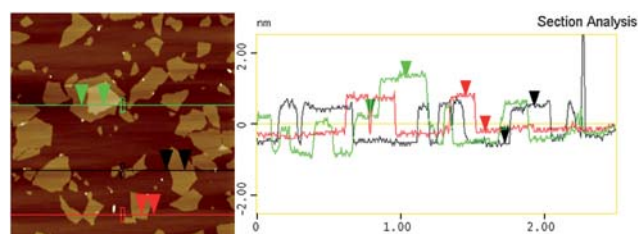


**Fig. 1** Tapping mode AFM analysis of graphite oxide sheets after sonication, showing platelets surface topography (left) and average thickness (right).

different degrees of oxygen removal and reformation of double bonds. The maximum conductivity ( $5500 \text{ S m}^{-1}$ ) was achieved for 72 h reduction time, after which no increase was observed anymore.

The sonication process, which drives the redispersion of Gr/PSS aggregates, can easily be monitored by UV–Vis spectroscopy. The maximum achievable exfoliation (which does not mean that 100% of platelets are effectively exfoliated) corresponds to the maximum achievable UV–Vis absorbance of the filler dispersion. The reasoning behind this statement is that individualized and very thin graphene sheets exhibit a UV–Vis absorption spectrum whereas bundled or stacked sheets do not. The absorbance increases continuously with increasing sonication energy-input. Time and energy provided for maximum exfoliation of Gr/PSS vary usually from 30 min to 1 h, which corresponds to 30 000–60 000 J, respectively.

After the maximum obtainable exfoliation was achieved, the dispersion of Gr/PSS was mixed with polystyrene latex, followed by freeze–drying and compression molding, resulting in a composite film. For clarity, the entire process is illustrated in Fig. 2.

The electrical conductivity of the nanocomposites as a function of the nanofiller content is shown in Fig. 3. At low graphene concentrations, as long as no conductive network of nanoplatelets is formed in the PS matrix, the conductivity of the nanocomposites remains very close to the conductivity value of the pure insulating PS matrix. The composites exhibit a conductivity percolation threshold when the filler content is still below 0.8 wt%. At concentrations between 0.9 and 1.2 wt% the conductivity increases drastically up to  $2 \text{ S m}^{-1}$ . At higher graphene loadings of about 2 wt%, the conductivity level is *ca.*  $15 \text{ S m}^{-1}$ , which is, to the best of our knowledge, the highest value measured for Gr/PS nanocomposites with low graphene loadings. MWD (molecular weight distribution) of the matrix material can strongly affect the percolation threshold of a nanofiller within PS matrix. For instance for carbon nanotubes,

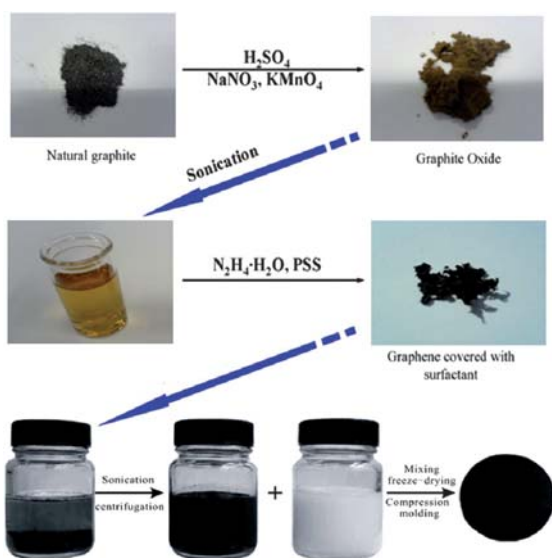


**Fig. 2** Schematic description of the multi-step process for preparation of graphene/polymer composites using latex technology. (PSS; poly(styrene sulfonate),  $70\,000 \text{ g mol}^{-1}$ ).

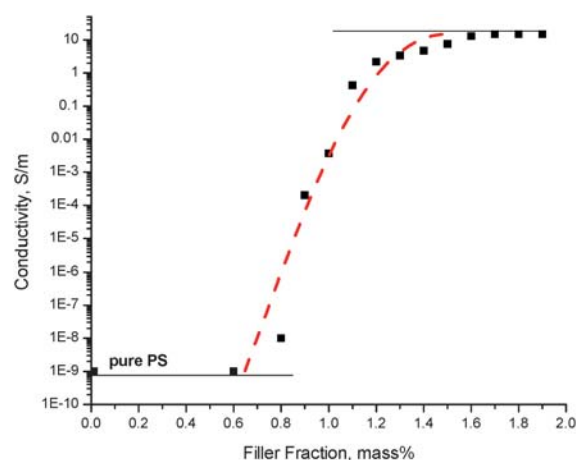


**Fig. 3** Electrical conductivity of graphene/PS composites as a function of graphene weight fraction. Values represent an average of 10 measurements on the sample; standard deviation is below 10%.

a significant decrease in the percolation threshold was observed upon the introduction of low molecular weight polymer, the shift being most pronounced for higher amounts of low molar mass polymer. The origin of this effect can be twofold: changes in MWD lead to rheological changes of the melt (*i.e.* decrease in melt viscosity) and low molecular weight polymer may replace surfactant from the carbon nanotubes surface (thereby changing the inter-tube distances and/or electrical conduction across junctions).<sup>27</sup> In this work, as mentioned before, high molecular weight PS latex was used with  $M_w 944 \text{ kg mol}^{-1}$ .

Table 1 compares conductive properties of graphene/nanotubes nanocomposites obtained *via* latex technology, using PS latex with the same MWD and using similar processing conditions.

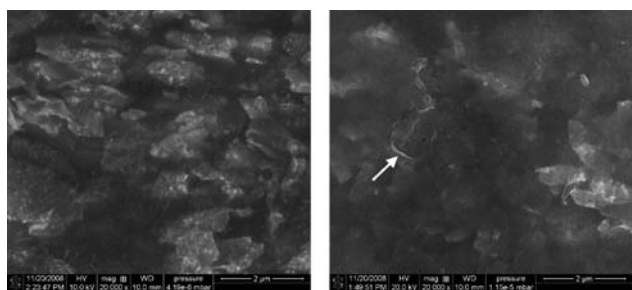
For the final application of graphene in nanocomposites, detailed knowledge of platelets dispersion and organization in the polymer matrix is most important to understand the properties and performance of the nanocomposites. To obtain this information, we have applied various microscopic techniques.

Fig. 4 shows a charge contrast SEM image of the surface of a Gr/PS composite film with a graphene concentration of 1.9 wt%. Besides a more or less dark background, bright areas are visible, which represent graphene sheets distributed in the polymer matrix. Because of the different capability for charge transport of the conductive graphene and the insulating polymer matrix, the secondary electron yield is enriched at the location of the graphene, which results in the contrast between the graphene network and the polymer matrix.<sup>22</sup>

Therefore, using charge contrast imaging at high acceleration voltage, we were able to gain representative information on the

**Table 1** Conductive properties of nanocomposites produced *via* latex technology

Nanofiller	Graphene	MWCNT	
		SWCNT	(Long) MWCNT
<b>Percolation threshold, wt%</b>	0.6	0.4 <sup>28</sup>	0.15 <sup>29</sup>
<b>Ultimate conductivity, <math>\text{S m}^{-1}</math></b>	15	20 <sup>28</sup>	13 <sup>30</sup>



**Fig. 4** High-resolution SEM charge contrast showing fairly straight and bended graphene sheets. The filler concentration is 1.9 wt%. Attention should be paid to curved lateral cross section sheets (marked by arrow), and to the different brightness of the graphene. Scale bar is 2  $\mu\text{m}$  in both images.

three-dimensional organization of a conductive network of graphene sheets in a polymer matrix. The brightness variations visible in the SEM charge contrast images can be related to the position of the graphene in the sample: high brightness means a position of the sheets at or near the surface, whereas sheets located deep in the nanocomposite appear darker.<sup>23</sup>

The local organization of graphene sheets in the conductive Gr/PS nanocomposites and their conductivity distribution has been also analyzed with nanometre resolution by means of conductive atomic force microscopy (C-AFM). Using a conductive AFM probe, in our case a gold-coated silicon tip, the local electrical conductivity can be measured at exactly the same area of the specimen subsequent to the topography and phase contrast imaging. The C-AFM tip measures the current throughout the volume of the nanocomposite specimen at a given voltage which is running *via* the graphene network to the ground contacts. Only platelets that are connected with the ground contacts can be monitored, and the observed differences in current are determined by the intra-network graphene junctions with highest resistivity. Graphene contributing to sub-networks without connection to the ground contacts show no current. In this way, a current distribution image is obtained and the conductive platelets can be distinguished from the insulating polymer matrix. Fig. 5 shows that most of the bright (white) areas corresponding to graphene in the cross-section topographic image (left) fit with the higher current level seen on the right mapping, indicating the presence of conductive pathways. The analyses of several images show that these networks were

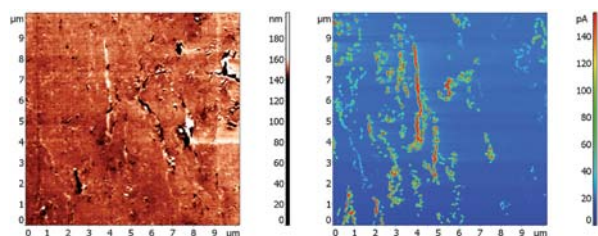


**Fig. 5** C-AFM images of the PS/graphene samples containing 1.9 wt% graphene obtained in topography (left), and as electrical current distribution image (right), showing the graphene platelets that are connected with the ground electrode.

observed mainly in the central region of the cross-sections if compared to the edges.

## Conclusions

For the first time highly conductive graphene/PS nanocomposites with a low percolation threshold have been prepared by latex technology.

The study demonstrates that it is possible to apply latex technology for the preparation of graphene-based nanocomposites. PSS-covered graphene platelets were successfully prepared *via* a known oxidation/reduction method and dispersed in water by means of sonication. PSS stabilizes the platelets and prevents their aggregation, but at the same time, because of its bulkiness and non-conductive character, probably limits the electron transport at the graphene junctions in the final nanocomposites.

Atomic force microscopy (AFM) shows that the thickness of the oxidized graphite platelets is around 1 nanometre, indicating approximately 2–3 graphene layers. Relatively well-dispersed graphene sheets in a PS matrix could be visualized using a high charge contrast scanning electron microscopy (SEM) imaging technique. Probably due to the application of the relatively new latex technology the distribution and homogeneity of the graphene filler inside the polymer could be improved in comparison to other standard nanocomposite manufacturing techniques.

The final conductivities of the Gr/PS nanocomposites, obtained by both four point and local current measurement techniques, reveal interestingly high values up to  $15 \text{ S m}^{-1}$ , which can be achieved for low nanofiller loadings (1.6–2 wt%). A pronounced percolation threshold exhibiting a quite low value around 0.8–0.9 wt% was observed for the produced PS/graphene nanocomposites.

## Notes and references

- 1 A. K. Geim and K. S. Novoselov, *Nat. Mater.*, 2007, **6**, 183–191.
- 2 C. Lee, X. Wei, J. W. Kysar and J. Hone, *Science*, 2008, **321**, 385–388.
- 3 M. J. McAllister, J. Li, D. H. Adamson, H. C. Schniepp, A. A. Abdala, J. Liu, M. Herrera-Alonso, D. L. Milius, R. Car, R. K. Prud'homme and I. A. Aksay, *Chem. Mater.*, 2007, **19**, 4396–4404.
- 4 S. Stankovich, D. A. Dikin, G. H. B. Dommett, K. M. Kohlhaas, E. J. Zimney, E. A. Stach, R. D. Piner, S. T. Nguyen and R. S. Ruoff, *Nature*, 2006, **442**, 282–286.
- 5 T. Ramanathan, S. Stankovich, D. A. Dikin, H. Liu, H. Shen, S. T. Nguyen and L. C. Brinson, *J. Polym. Sci., Part B: Polym. Phys.*, 2007, **45**, 2097–2112.
- 6 J. J. Mack, L. M. Viculis, A. Ali, R. Luoh, G. L. Yang, H. T. Hahn, F. K. Ko and R. B. Kaner, *Adv. Mater.*, 2005, **17**, 77–80.
- 7 Y. Si and E. T. Samulski, *Nano Lett.*, 2008, **8**, 1679–1682.
- 8 R. Muszynski, B. Seger and P. V. Kamat, *J. Phys. Chem. C*, 2008, **112**, 5263–5266.
- 9 S. Stankovich, R. D. Piner, X. Chen, N. Wu, S. T. Nguyen and R. S. Ruoff, *J. Mater. Chem.*, 2006, **16**, 155–158.
- 10 K. S. Novoselov, A. K. Geim, S. V. Morozov, D. Jiang, M. I. Katsnelson, I. V. Grigorieva, S. V. Dubonos and A. A. Firsov, *Nature*, 2005, **438**, 197–200.
- 11 K. S. Novoselov, S. V. Morozov, T. M. G. Mohinddin, L. A. Ponomarenko, D. C. Elias and R. Yang, *Phys. Status Solidi B*, 2007, **244**, 4106–4111.
- 12 K. S. Novoselov, A. K. Geim, S. V. Morozov, D. Jiang, Y. Zhang, S. V. Dubonos, I. V. Grigorieva and A. A. Firsov, *Science*, 2004, **306**, 666–669.

- 
- 13 K. Wakabayashi, C. Pierre, D. A. Dikin, R. S. Ruoff, T. Ramanathan, L. C. Brinson and J. M. Torkelson, *Macromolecules*, 2008, **41**, 1905–1908.
  - 14 K. S. Kim, Y. Zhao, H. Jang, S. Y. Lee, J. M. Kim, J. H. Ahn, P. Kim, J. Y. Choi and B. H. Hong, *Nature*, 2009, **457**, 706–710.
  - 15 G. Eda, G. Fanchini and M. Chhowalla, *Nat. Nanotechnol.*, 2008, **3**, 270–274.
  - 16 T. Sekitani, Y. Noguchi, K. Hata, T. Fukushima, T. Aida and T. Someya, *Science*, 2008, **321**, 1468–1472.
  - 17 O. Regev, P. N. B. ElKati, J. Loos and C. E. Koning, *Adv. Mater.*, 2004, **16**, 248–251.
  - 18 N. Grossiord, J. Loos and C. E. Koning, *J. Mater. Chem.*, 2005, **15**, 2349–2352.
  - 19 N. Grossiord, J. Loos, O. Regev and C. E. Koning, *Chem. Mater.*, 2006, **18**, 1089–1099.
  - 20 J. Yu, K. Lu, E. Sourty, N. Grossiord, C. E. Koning and J. Loos, *Carbon*, 2007, **45**, 2897–2903.
  - 21 W. S. Hummers and R. E. Offeman, *J. Am. Chem. Soc.*, 1958, **80**, 1339.
  - 22 J. Loos, A. Alexeev, N. Grossiord, C. E. Koning and O. Regev, *Ultramicroscopy*, 2005, **104**, 160–167.
  - 23 M. Ouyang, J. L. Huang, C. L. Cheung and C. M. Lieber, *Science*, 2001, **292**, 702–705.
  - 24 J. R. Yu, N. Grossiord, C. E. Koning and J. Loos, *Carbon*, 2007, **45**, 618–623.
  - 25 N. Grossiord, O. Regev, J. Loos, J. Meuldijk and C. E. Koning, *Anal. Chem.*, 2005, **77**, 5135–5139.
  - 26 A. Alekseev, A. Efimov, K. Lu and J. Loos, *Adv. Mater.*, 2009, **21**, 4915–4919.
  - 27 M. C. Hermant, N. M. B. Smeets, R. C. F. van Hal, J. Meuldijk, H. P. A. Heuts, B. Klumperman, A. M. van Herk and C. E. Koning, *e-Polymers*, 2009, 22.
  - 28 M. C. Hermant, B. Klumperman, A. V. Kyrlyuk, P. van der Schoot and C. E. Koning, *Soft Matter*, 2009, **5**, 878–885.
  - 29 N. Grossiord, J. Loos, L. van Laake, M. Maugey, C. Zakri, C. E. Koning and J. Hart, *Adv. Funct. Mater.*, 2008, **18**, 3226–3234.
  - 30 J. Yu, K. Lu, E. Sourty, N. Grossiord, C. E. Koning and J. Loos, *Carbon*, 2007, **45**, 2897–2903.